J Glob Optim (2007) 37:527–539
DOI 10.1007/s10898-006-9060-x

ORIGINAL ARTICLE

A population global optimization algorithm to solve the image alignment problem in electron crystallography

P. M. Ortigosa · J. L. Redondo · I. García · J. J. Fernández

Received: 19 May 2006 / Accepted: 22 May 2006 / Published online: 9 August 2006

Abstract Knowledge of the structure of biological specimens is critical to understanding their function. Electron crystallography is an electron microscopy (EM) approach that derives the 3D structure of specimens at high-resolution, even at atomic detail. Prior to the tomographic reconstruction, the images taken from the microscope have to be properly aligned. Traditional alignment methods in electron crystallography are based on a phase residual function to be minimized by inefficient exhaustive search procedures. This work addresses this minimization problem from an evolutionary perspective. Universal Evolutionary Global Optimizer (UEGO), an evolutionary multimodal optimization algorithm, has been applied and evaluated for the task of image alignment in this field. UEGO has turned out to be a promising technique alternative to the standard methodology. The alignments found out by UEGO show high levels of accuracy, while reducing the number of function evaluations by a significant factor with respect to the standard method.

Keywords Evolutionary algorithms · Global optimization · Stochastic optimization · Image alignment · Electron microscope tomography · Electron crystallography

1 Introduction

High-resolution structural information is essential for understanding the function of biological specimens. This is a crucial subject of research in molecular biology and related biosciences. Electron microscope (EM) tomography allows the investigation of structure of specimens over a wide range of resolutions, from subcellular level up to atomic detail [2, 7, 14]. In EM tomography, a set of images taken from the specimen

P. M. Ortigosa (✉) · J. L. Redondo · I. García · J. J. Fernández
Department of Computer Architecture and Electronics, University of Almería,
04120 Almería, Spain
e-mail: ortigosa@ual.es

J. J. Fernández
e-mail: jjfdez@ual.es

at different tilts and orientations is combined by tomographic reconstruction methods to yield the structure. Since the acquired EM images are not mutually aligned, an alignment procedure has to be applied prior to the reconstruction process. This work is focused on electron crystallography [16, 20, 21], currently the only approach capable of reaching atomic resolution by EM of crystallized biological specimens [8, 10, 12]. In this approach, the problem is limited to translational alignment and the standard alignment method is based on the minimization of a error function by means of inefficient exhaustive search procedures [1, 5, 6, 9, 21].

In this work, image translational alignment in electron crystallography is addressed in an evolutionary framework. The error function involved in this problem is used as an objective function to be minimized by a stochastic optimizer. This is a multimodal optimization problem as the number of local minima may be large. The optimizer must thus find out the global optimum under the presence of many deceptive optima. In this work, an evolutionary multimodal optimization algorithm, the *Universal Evolutionary Global Optimizer* (UEGO, [13]), is evaluated.

In multimodal optimization, the optimizer should discover the structure of the local optima to reach the global optimum. Time should thus be spent in discovering new and promising regions rather than exploring the same region multiple times. The UEGO uses a non-overlapping set of clusters, which define sub-domains of the search space. As the algorithm progresses, the search process can be directed toward smaller regions by creating new sets of non-overlapping clusters defining smaller sub-domains. This process is a kind of cooling method similar to simulated annealing. A particular cluster is not a fixed part of the search domain; it can move through the space as the search proceeds. The non-overlapping property of the set of clusters is maintained however. The UEGO is abstract in the sense that the 'cluster-management' and the cooling mechanism has been logically separated from the optimization algorithm. Therefore, any kind of optimizer can be used to work inside a cluster, and here a stochastic hill climber [15] has been used.

2 Description of the evolutionary optimization algorithm: universal evolutionary global optimizer

A key notion in UEGO is that of a *species*. A species is equivalent to an *individual* in a usual evolutionary algorithm. A species can be thought of as a window (or cluster) on the whole search space (Fig. 1).

This window is defined by its *center*, which is a solution, and a *radius*. The algorithm evolves creating as many windows (with different radii values) as local optima the objective function has. This set of clusters or *species_list* would be equivalent to the term population in an classical evolutionary algorithm. The maximal length of the species list is given by *max_spec_num* (the maximum population size).

This definition of species assumes a *distance* defined over the search space. In the algorithm, any kind of distance can be defined depending on the properties of the optimization problem. By default, UEGO uses the hamming distance for combinatorial problems, and the euclidean distance for problems defined in real domains.

The mutation of an species consists in calling a local optimizer that will try to find a solution better than the center of the species. When the optimizer is called by a species, it can 'see' only the window of that species, in such a way that any single step made by the optimizer in a given species is no larger than the radius of that species.

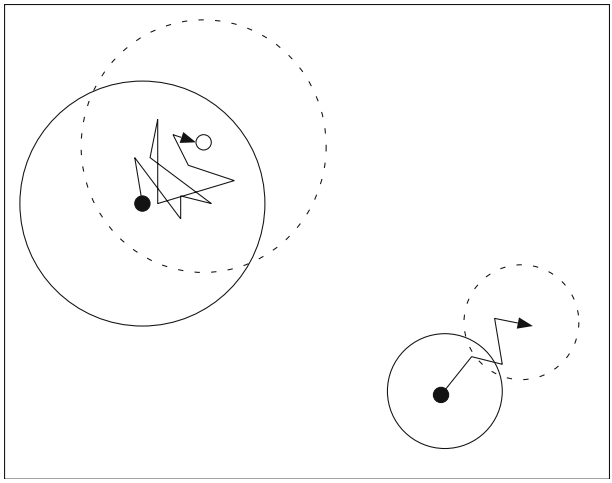

Fig. 1 Concept of species

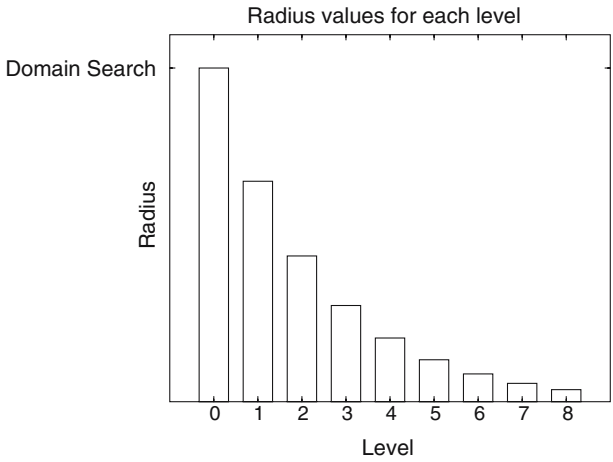

Fig. 2 Radius values for the levels based on an exponentially decreasing function

If the value of a new solution found by the optimizer is better than that of the old center, the new solution becomes the center and the window is moved while it keeps the same radius value.

The radius of a species is not arbitrary; it is taken from a list of decreasing radii, the *radius list*, that follows a *cooling schedule* (see Fig. 2). The first element of this list is the diameter of the search space. If the radius of a species is the ith element of the list, then the *level* of the species is said to be i. Given the smallest radius and the largest one (r_l and r_1), the radii in the list are expressed by the exponential function

$$r_i = r_1 \left(\frac{r_l}{r_1}\right)^{\frac{i-1}{l-1}}, \quad (i = 2, \ldots, l). \tag{1}$$

The parameter *levels* indicates the maximal number of levels in the algorithm, i.e. the number of different 'cooling' stages. Every level i (with $i \in [1,levels]$) has a radius value (r_i) and two maxima on the number of function evaluations (FE) namely new_i (maximum FE allowed when creating new species) and n_i (maximum FE allowed when optimizing individual species).

2.1 Input parameters

In UEGO the most important parameters are those defined at each level: the radii (r_i) and the maximum number of function evaluations for species creation (new_i) and optimization (n_i). These parameters are computed from a set of input global parameters:

(1) evals (N): The maximal number of function evaluations for the whole optimization process. Note that the actual number of function evaluations is usually less than this value.
(2) *levels* (l): The maximum number of levels, i.e. the number of cooling stages.
(3) *max_spec_num* (M): The maximum length of the species list or the maximum allowed population size.
(4) *min_r* (r_l): The radius that is associated with the maximum level, i.e. *levels*.

An in-detail description of these input parameters and their relationship to the parameters at each level (r_i, new_i, n_i) can be found in [13].

2.2 The Algorithm

The UEGO algorithm has the following structure:

```
Begin UEGO
    Init_species_list
    Optimize_species(n_1)
    for i = 2 to levels
        Determine r_i, new_i, n_i
        Create_species(new_i/length(species_list))
        Fuse_species(r_i)
        Shorten_species_list(max_spec_num)
        Optimize_species(n_i/max_spec_num)
        Fuse_species(r_i)
    end for
End UEGO
```

In the following, the different key stages in the algorithm are described as follows:

(1) *Init_species_list:* A new species list consisting of one species with a random center at level 1 is created.
(2) *Create_species(evals):* For every species in the list, random trial points in the 'window' of the species are created, and for every pair of trial points the objective function is evaluated at the middle of the *section* connecting the pair (see Fig. 3). If the value in the middle point is worse than the values of the pair, then the members of the pair are inserted in the species list. Every newly inserted species is assigned the actual level value (i).

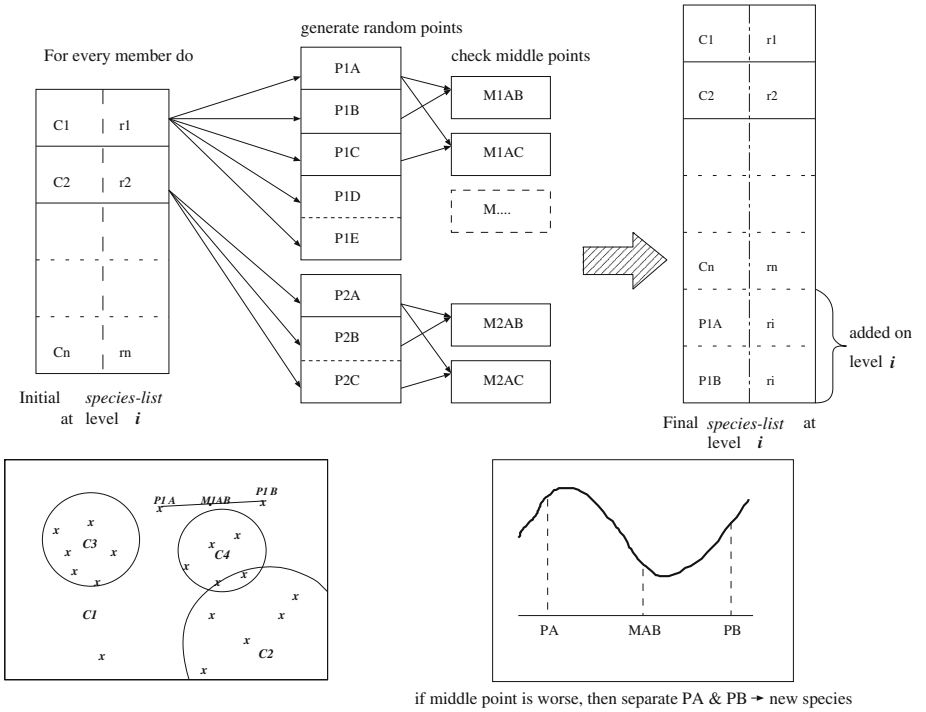

Fig. 3 Creation procedure

As a result of this procedure the species list will eventually contain several species with different levels (hence different radii). The motivation behind this method is to create species that are on different 'hills' so ensuring that there is a valley between the new species. The parameter of this procedure (*evals*) is an upper bound of the number of function evaluations. Note that this algorithm needs a definition of section in the search space. In terms of genetic algorithms, it could be thought that, in this procedure, a single parent (*species*) is used to generate offspring (*new species*), and all parents are involved in the procedure of generating offspring.

(1) *Fuse_species*(*radius*)*:* If the centers of any pair of species from the species list are closer to each other than the given radius, the two species are fused (see Fig. 4). The center of the new species will be the one with the better function value while the level will be the minimum of the levels of the original species (so the radius will be the largest one).

(2) *Shorten_species_list*(*max_spec_num*)*:* It deletes species to reduce the list length to the given value. Higher level species are deleted first, therefore species with larger radii are always kept. For this reason one species at level 1 whose radius is equal to the diameter of the search domain always exists, making it possible to escape from local optima.

(3) *Optimize_species*(*budget_per_species*)*:* It executes the optimizer for every species with a given number of evaluations (*budget_per_species*) (see Fig. 1). At level i, the budget_per_species is computed as n_i/max_spec_num, i.e., it depends on the maximum species number or maximum population.

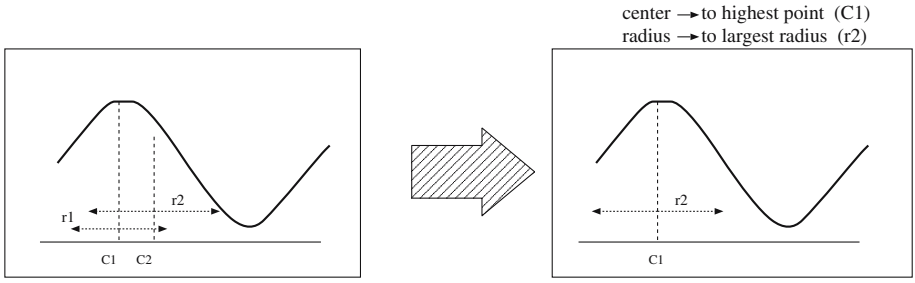

Fig. 4 Fusion procedure

Note that UEGO may terminate simply because it has executed all of its levels. The final number of function evaluations thus depends on the complexity of the objective function. This is qualitatively different from genetic algorithms, which typically run up to a limit on the number of function evaluations.

3 Image alignment in electron crystallography

The combination of information from different EM images taken with the specimen at distinct tilts and orientations is central to the process of 3D reconstruction [2]. These starting EM images are not, in general, mutually aligned as a result of the particular orientation of each specimen and the scanning process. This involves that the initial images have arbitrary phase origins in the Fourier domain. An essential prior step before the reconstruction is a proper alignment so that the images have a common phase origin. Only then, the 3D reconstruction process can be carried out to derive the 3D structure of the specimen under study. The alignment stage is thus paramount. In practice, EM images are severely corrupted by noise, deformations and other measurement errors which turn the alignment into an optimization problem.

This work is focused on electron crystallography, the only approach in electron microscopy capable of reaching atomic resolution [7, 8, 10, 12]. In this approach, biological specimens are crystallized to form 2D crystals [16, 20, 21]. These crystals are made up of tens of thousands of units of the same specimen arranged in a regular manner [4]. When processing images of such objects, Fourier transformation is usually employed. So, in electron crystallography, the images are processed and combined using a discrete number of indexed Fourier components [1, 9, 17]. Figure 5 sketches the process of extraction and indexing of the Fourier components of an image in electron crystallography. Figure 5 (upper left) shows an image of a 2D crystal composed by a ordered repetition of a specimen. This can be considered as the convolution of a lattice with a specimen. Therefore, the Fourier transform (FT) of the image is the product of the FT of the specimen with the FT of the lattice, and the latter proves to be another lattice: the Fourier lattice. Consequently, there only are a discrete set of Fourier components that are meaningful from the structural point of view: those ones located in the Fourier lattice (Fig. 5, upper right). They are then extracted and indexed (same figure, lower left). They turn out to be the Fourier components of the average unit that is repeated across the 2D crystal [9]. This average unit can be computed by Fourier synthesis from the corresponding indexed Fourier components (Fig. 5, lower

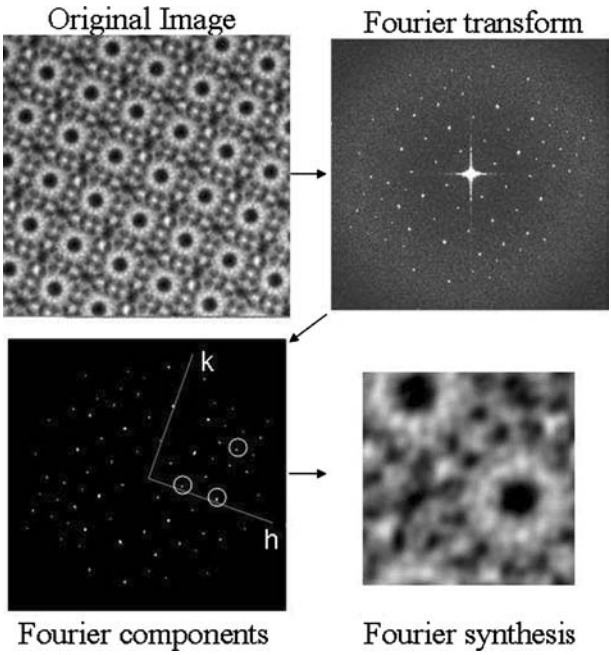

Fig. 5 Analysis of crystal images into Fourier components. The FT of the image has the meaningful components located at the Fourier lattice. These components are then extracted and indexed with indices (h, k). In the figure, the components with indices $(2, 0)$, $(4, 0)$, and $(4, 4)$ are marked with *circles*. The average unit in the crystal is obtained by Fourier synthesis from the extracted components

right). The images shown hereafter represent the average specimen computed by synthesis from the Fourier components of the corresponding crystal.

The need of image alignment in electron crystallography is limited to translational alignment. This simplification comes from the fact that the Fourier components of all the images are accordingly indexed [9] and hence the rotational alignment is implicitly carried out.

There is a wealthy literature about image alignment methods (for instance, see [3, 11] for reviews of registration techniques). For image translational alignment, the classic methods are based on cross-correlation functions [3, 11]. However, the fact that the cross-correlation function is, in general, strongly influenced by low-resolution frequency components makes it inappropriate for high-resolution structural analyses by EM. As electron crystallography is aimed to reach ultrahigh—even atomic—resolution, those methods were discarded long time ago in favor of methods that ignore the relative weighting among the frequency components [1, 5, 6, 9]. In electron crystallography, image translational alignment has been traditionally performed by minimizing a phase residual function which is directly derived from the spatial shift property of the FT [1, 5, 9, 6]:

$$PR(x, y) = \frac{1}{n} \sum_i |(\phi_{\text{ref}}(u_i,\ v_i) - (\phi(u_i,\ v_i) - (u_i x + v_i y))) \ \text{MOD}\ 360^\circ| \qquad (2)$$

where x and y are the phase shifts (in degrees) along X and Y-axes, respectively; $\phi_{\text{ref}}(u_i,\ v_i)$ the phase of the frequency component $(u_i,\ v_i)$ the reference image(s);

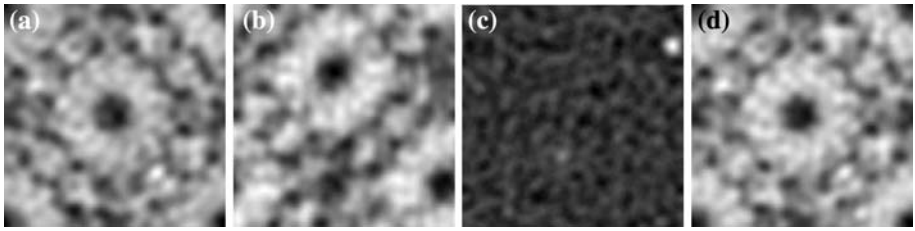

Fig. 6 Traditional alignment method in electron crystallography. **(a)** Reference image. **(b)** Image to be aligned. **(c)** Phase residual map. **(d)** Average image resulting from the alignment of image in **(b)** and merging with the image in **(a)**.

$\phi(u_i,\ v_i)$ the phase of the frequency component $(u_i,\ v_i)$ the image to be aligned to the reference; and n the total number of frequency components in this comparison. Note that the frequency terms u_i and v_i are computed from the corresponding indexes h and k after the corresponding conversion index-to-frequency (Å^{-1}).

The alignment of a new image with respect to a reference image essentially consists of determining the global minimum of the phase residual function. This minimization is traditionally carried out by means of an inefficient exhaustive search procedure that evaluates all the possible shifts in a discrete search space [1, 5, 6, 9, 21]. The alignment of the new image is then accomplished by applying the phase shift (x, y) with the lowest phase residual.

Figure 6 shows an example of alignment with images from ϕ29-phage connector [18] obtained by electron microscopy of 2D crystals. The reference image is shown in Fig. 6a and an image to be aligned in Fig. 6b. These images represent the average specimen in the crystals, and were computed by Fourier synthesis. The phase residual map in Fig. 6c shows the PR function with 361×361 samples at intervals of 1° in either direction X or Y. The upper left corner of the map corresponds to a shift of $(x,\ y) = (-180°, -180°)$. The lower right corner corresponds to $(x,\ y) = (+180°, +180°)$. White levels in the error map represent low-values, whereas black levels denote high values. The search of the global minimum was performed with a precision of 0.1°, and was found at (162.5°, −113.1°). Fig. 6d shows the average image resulting from the merging of the aligned image and the reference.

In practice, this exhaustive search process is carried out hierarchically. First, the whole search space (360° in X and 360° in Y) is discretized at intervals of 3° and the minimum is sought in that discrete space. Afterward, the search is progressively refined around that minimum with decreasing resolutions (1.0°, 0.1°, etc). At the end, this approach is able to yield the global optimum with a precision of 0.01° using 43,200 evaluations. This heuristic multi-level search approach works because the local minima exhibited by the phase residual function are not, in general, extremely sharp.

4 Experiments

This work is intended to evaluate the application of UEGO to the translational image alignment problem in electron crystallography. Essentially, our approach for alignment consists of minimizing the phase residual function $PR(x, y)$ by means of UEGO. The hypothesis to test is that our approach is able to reach the global minimum of the error function using less function evaluations than the standard approach.

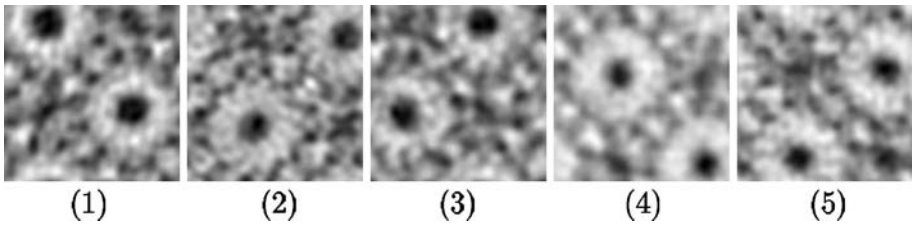

Fig. 7 EM images of $\phi 29$ connectors that have been used in this work

The proposed approach was tested and evaluated over five EM images of $\phi 29$-bacteriophage connectors obtained from 2D crystals. Bacteriophage connectors, which play an essential role in viral morphogenesis, are typically used to study the protein–protein and protein–nucleic acid interactions in structural biology [18, 19]. The five images of $\phi 29$-bacteriophage connectors were already used in previous structural analyses of this specimen, in particular in the determination of its 3D structure [18]. These images had significant structural information up to 10 Å resolution, as assessed by [18]. Figure 7 shows the average specimens repeated across the corresponding crystals. These averages were obtained by means of Fourier synthesis from the Fourier components of the crystals, as described above. Due to the stochastic nature of UEGO, all the numerical results given in this work are average values of a hundred executions, obtaining an statistic ensemble of experiments. From this data set, average values of the different metrics (number of function evaluations, phase shifts, phase residual, etc.) and the corresponding confidence intervals at 95% were computed.

Our experimental methodology can be split into two stages: the first stage of training was intended to determine the values of the free parameters of UEGO which produce good solutions for the translational alignment problem in electron crystallography; the second stage of testing was designed for evaluating the efficiency and effectiveness of UEGO in finding the global solution, and for comparing to the traditional method.

4.1 Training universal evolutionary global optimizer

This stage was intended to determine the optimal parameters of UEGO for this problem. [13] introduced UEGO and stated that a robust parameter setting consists of a large enough number of levels (l), a relatively small minimum radius (r_l), a sufficient maximum number of species (M) and a large value of N in order to get a minimum budget per species, which is sufficient in the optimization process.

The five EM images just presented were used. Each test image was subjected to random shifts to generate an ensemble of five synthetic shifted images. The experiments were designed to find out the UEGO parameters that yielded the alignment of the synthetic images with respect to the corresponding original image in an optimal way, in terms of number of evaluations and phase residual. The values of the parameters tested are shown in Table 1. Experiments were performed for all combinations of these parameter settings. Every set of parameters was evaluated 2,500 times (25 synthetic images, 100 executions).

The experiments in this stage showed that UEGO does not get trapped in local optima when the number of levels is high-enough ($l = 10$), hence the cooling process

Table 1 Values of the UEGO parameters that were tested in the training stage

Max_No_funct-_evals (N)	Levels (l)	Max_spec_num (M)	Min_r (r_l)
100,000, 300,000	5, 8, 10	20, 30	1, 3, 5
500,000, 1,000,000	15	50, 100	8, 10

allows the algorithm to escape from local optima. When the number of levels is too high, the process is too slow and the algorithm does not finish the optimization process, so it requires a larger value for N.

For fixed values of l and r_l, the results showed that there is a tendency to find more species (optima) as M increases. This increment of species can be explained by the fact that a larger population size is allowed and hence, it turns out to be easier to explore the search space. However, for those fixed parameters, the number of function evaluations decreases as M increases, owing to the decrease in the budget per species (n_i/M) in the optimization process.

With regard to the final radius, it was observed that the smaller radii, the more accurate solutions. However, there is a higher risk of being trapped in local minima. The results showed that for a fixed value of M and l, the number of detected species (optima) increases as the radius (r_l) decreases. This growth of species lies in the fact that the number of fused species decreases when the radii are smaller. Since each species had been assigned a certain maximum of function evaluations (budget per species) in the optimization process, the more species there are, the more function evaluations are consumed. Consequently, the number of function evaluations also increases as the radius decreases. In summary, there is a tradeoff among high accuracy in the solutions, the risk of being trapped in local minima and the number of function evaluations.

The optimal parameters that were finally found consisted of $N = 300,000$, $l = 10$, $M = 30$, and $r_l = 8$. This set of parameters yielded an average number of function evaluations of 23730 ± 163, and a negligible average phase residual of $0.00051° \pm 0.000058°$.

4.2 Assessment of UEGO in electron microscope tomography

This stage was aimed to evaluate UEGO for experimental alignment problems in electron crystallography. The robust parameter settings deduced above were used. The five experimental EM images from $\phi 29$ connectors above presented were used. All possible alignments between pairs of images were carried out, resulting in 20 tests. For the sake of comparison, both methods, UEGO and the traditional one, were evaluated in terms of number of function evaluations and phase residual.

Average results and confidence intervals for UEGO were computed considering the 20 tests and 100 executions per test. The average number of evaluations resulted in $24,930 \pm 217$. The heuristic rule for the standard method was used, resulting in 43,200 evaluations in all the alignments. The differences in phase residual between the results of both methods were negligible. Accordingly, the phase origins found by both proved to be very close, with differences in the order of $0.001°$. Therefore, these experiments have shown that UEGO is able to reduce the number of function evaluations by a factor around 43% while maintaining the same levels of phase residual.

Table 2 Results for alignment using UEGO

Ref	1		2		3		4		5	
	FE	PR	FE	PR	FE	PR	FE	PR	FE	PR
1	–	–	24,311	25.36	24,607	34.42	25,436	40.05	25,576	31.92
2	24,457	25.36	–	–	24,407	39.30	25,201	46.73	24,683	33.06
3	24,527	34.42	24,357	39.30	–	–	24,942	45.29	24,595	41.14
4	25,423	40.05	24,995	46.73	25,042	45.29	–	–	25,549	20.15
5	25,566	31.92	24,589	33.06	24,687	41.14	25,650	20.15	–	–

Table 3 Phase residual of the aligned images with respect to the average aligned image

	Image No 1	Image No 2	Image No 3	Image No 4	Image No 5
P.R.:	20.92°	17.48°	23.96°	30.39°	19.64°

Table 2 summarizes the results obtained with UEGO. The first row of the table indicates the index of the image (see Fig. 7) that was used as a reference in the tests. The corresponding column then presents the results of the alignment of the remaining images with respect to the reference. The results consist of the number of FE that was finally required ('FE'), and the value (in degrees) of the phase residual function found at the global minimum ('PR'). Note that the alignment of two images should yield the same results, whatever image is used as the reference. However, as UEGO is a stochastic algorithm, the number of function evaluations may not be exactly the same. That can be seen in that table. For instance, see the alignment of image No 1 with respect to image No 2, and the one of image No 2 with respect to image No 1. The phase residual at the global minimum is 25.36° in both cases, but the number of evaluations is slightly different.

An additional test was then carried out in order to further compare both alignment methods. The best of the five EM images was selected. This selection was accomplished based on the average phase residual in the tests above. The fifth image was selected, as its four tests (see column labelled with '5' in Table 2) yielded the lowest average PR, an average value of 31.57°. This image was then centered according to symmetry criteria [18] as Fig. 8a shows. The remaining images were then aligned with respect to it (Figs. 8b–e) and then averaged all together (Fig. 8f). The resulting average aligned image had better signal-to-noise ratio than the images by themselves, hence it represented a more reliably projection of the specimen. So, this test consisted of comparing all the independent aligned images (Fig. 8a–e) with the average image (Fig. 8f) in terms of phase residual. This scheme was applied for both alignment methods for comparison's sake. The same results in terms of phase residual were obtained. These results are presented in Table 3. With regard to the number of function evaluations, UEGO required 24575 ± 173 for each alignment whereas the standard method used 43,200. Therefore, this test confirmed that UEGO succeeds in reducing the number of function evaluations by a factor around 43% with no changes in the phase residual.

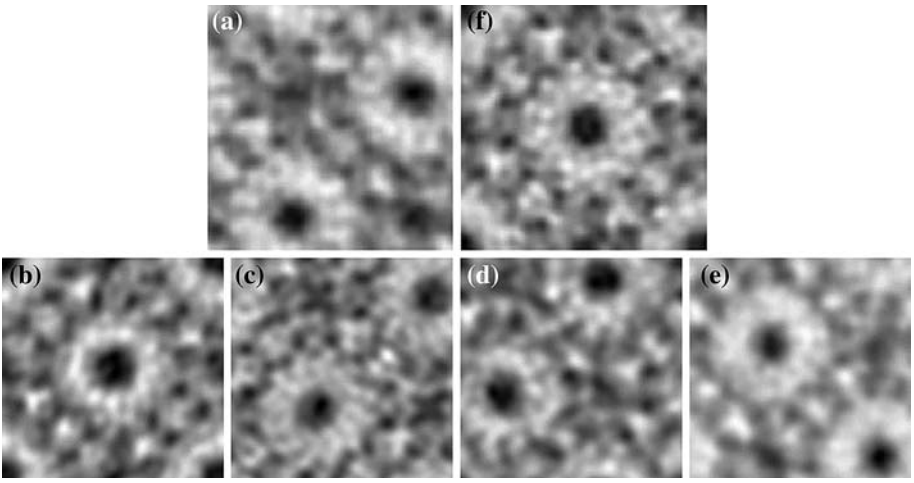

Fig. 8 Tests based on average aligned image. **(a)** The best image was centered and used as the reference. **(b–e)** the remaining images were then aligned with respect to it. **(f)** Average aligned image resulting from the average of **(a–e)**.

5 Conclusions

In this work the application of UEGO to image translational alignment in electron crystallography has been evaluated and compared to the standard methodology. The results have shown that UEGO succeeds in reducing the number of evaluations by a factor around 43% with respect to the traditional method.

The value and the precision of the phase origins found by UEGO are essentially the same as obtained by the standard method, hence the differences in phase residual are negligible. Therefore, we can conclude that UEGO exhibits the same performance as the standard method in terms of phase residual.

As far as the number of evaluations and the computation time are concerned, UEGO clearly outperforms the traditional method. This proves to be a significant advantage in electron crystallography since there may be several hundreds of images involved in a 3D reconstruction or any other typical structural analysis. Therefore, there is a substantial computation time spent in mutual image alignment and UEGO could then help to considerably reduce this burden.

The fact that UEGO must have its free parameters tuned to be fully exploited may imply a disadvantage. Fortunately, the optimal parameter setting has to be found only once for the problem at hand. Moreover, there exist some general guidelines for tuning UEGO parameters that were stated when the algorithm was introduced. Although the optimal values depend on the particular problem and a fine-tuning of the parameters is thus advizable, these general rules could be used to avoid this effort and get sub-optimal values of the parameters that yield good performance.

Acknowledgements The authors would like to thank Prof. Dr. J.M. Valpuesta who kindly provided the electron microscopy images of connectors of ϕ29-bacteriophage. This work has been partially supported by the Ministry of Education and Science of Spain through grants TIC2002-00228 and TIN2005-00447, Fundacion BBVA (BBVA-2004X578) and EU (3DEM - European Network of Excellence, EU-FP6-LSHG-CT-2004-502828).

References

1. Amos, L.A., Henderson, R., Unwin, P.N.T.: Three-dimensional structure determination by electron microscopy of two-dimensional crystals. Prog. Biophys. Mol. Biol. **39**, 183–231 (1982)
2. Baumeister, W., Steven, A.C.: Macromolecular electron microscopy in the era of structural genomics. Trends Biochem. Sci. **25**: 624–631 (2000)
3. Brown, L.G.: A survey of image registration techniques. ACM Comput. Surve. **24**, 325–376 (1992)
4. Fernandez, J.J., Carazo, J.M.: Analysis of structural variability within two-dimensional biological crystals by a combination of patch averaging techniques and self organizing maps. Ultramicroscopy, **65**, 81–93 (1996)
5. Grant, R.A., Schmid, M.F., Chiu, W., Deatherage, J.F., Hosoda, J.: Alignment and merging of electron microscope images of frozen hydrated crystals of the T4 DNA helix destabilizing protein gp32*I. Biophys. J. **49**, 251–258 (1986)
6. He, W.Z., Carazo, J.M., Fernandez, J.J.: A new phase consistency criterion and its application in electron crystallography. Ultramicroscopy, **85**, 73–91, (2000)
7. Henderson, R.: Realizing the potential of electron cryo-microscopy. Q. Rev. Biophys. **37**, 3–13 (2004)
8. Henderson, R., Baldwin, J.M., Ceska, T.A, Zemlin, F., Beckmann, E., Downing, K.H.: Model for the structure of bacteriorhodopsin based on high-resolution electron cryo-microscopy. J. Mol. Biol. **213**, 899–929 (1990)
9. Henderson, R., Baldwin, J.M., Downing, K.H., Lepault, J., Zemlin, F.: Structure of purple membrane from halobacterium halobium: recording, measurement and evaluation of electron micrographs at 3.5 å resolution. Ultramicroscopy, **19**, 147–178 (1986)
10. Kuhlbrandt, W., Wang, D.N., Fujiyoshi, Y.: Atomic model of plant light-harvesting complex by electron crystallography. Nature **367**, 614–621 (1994)
11. Maintz, J.B.A., Viergever, M.A.: A survey of medical image registration. Med. Image Anal **2**(1), 1–36 (1998)
12. Nogales, E., Wolf, S.G., Downing, K.H.: Structure of the alpha beta tubulin dimer by electron crystallography. Nature, **391**, 199–203 (1998)
13. Ortigosa, P.M., García, I., Jelasity, M.: Reliability and performance of UEGO, a clustering-based global optimizer. J. of Global Optim. **19**(3), 265–289 (2001)
14. Sali, A., Glaeser, R., Earnest, T., Baumeister, W.: From words to literature in structural proteomics. Nature **422**, 216–225 (2003)
15. Solis, F.J., Wets, R.J.B.: Minimization by random search techniques. Math. Oper. Res. **6**(1), 19–30 (1981)
16. Stahlberg, H., Fotiadis, D., Scheuring, S., Rémigy, H., T. Braun, Mitsuoka, K., Fujiyoshi, Y., Engel, A.: Two-dimensional crystals: a powerful approach to assess structure, function and dynamics of membrane proteins. FEBS Lett. **504**, 166–172 (2001)
17. Stewart, M.: Introduction to the computer image processing of electron micrographs of two-dimensionally ordered biological structures. J. Elec. Microsc. Tech. **9**, 301–324 (1988)
18. Valpuesta, J.M., Fernandez, J.J., Carazo, J.M., Carrascosa, J.L.: The three-dimensional structure of a DNA translocating machine at 10 Å resolution. Structure **7**, 289–296 (1999)
19. Valpuesta, J.M., Sousa, N., Barthelemy, I., Fernández, J.J. Fujisawa, H., Ibarra, B., Carrascosa, J.L.: Structural analysis of the bacteriophage t3 head-to-tail connector. J. Struct. Biol. **131**, 146–155 (2000)
20. Walz, T., Grigorieff, N.: Electron crystallography of 2D crystals of membrane proteins. J. Struct. Biol. **21**, 142–161 (1998)
21. Yeager, M., Unger, V.M., Mitra, A.K.: Three-dimensional structure of membrane proteins determined by 2D crystallization, electron cryomicroscopy, and image analysis. Methods Enzymol. **294**, 135–180 (1999)